ROYAL SOCIETY OF CHEMISTRY

Journal Name

ARTICLE TYPE

Downsizing the BAD BH3 peptide to small constrained α-helices with improved ligand efficiency[†]

Nicholas E. Shepherd,[*a] Rosemary S. Harrison,[a] Gloria Ruiz-Gomez,[a,b] Giovanni Abbenante,[a] Jody M. Mason[c] and David P. Fairlie[*a]

Bcl2 Homology (BH) proteins can either trigger or prevent programmed cell death or apoptosis. Deregulation of the BH protein family network leads to evasion of apoptosis, uncontrolled proliferation and is a hallmark of cancer. Inhibition of pro-survival BH proteins is a promising chemotherapeutic strategy for certain cancers. We have examined whether helix-constrained peptides based on the BAD BH3 domain (residues 103–127) can be downsized to much smaller more drug-like peptides. We report the preparation, structural characterisation, *in vitro* Bcl-xL inhibition and leukemic T-cell killing ability of 45 linear, mono-, bi- and tricyclic helical peptidomimetics between 8- and 19-residues in length. We show that the BAD BH3 can be downsized to 8–14 residues and still maintain appreciable affinity for Bcl-xL. In addition, the binding efficiency indices (BEI) of the downsized mimetics are significantly higher than the BAD BH3 and similar stapled BH3 mimetics, approaching drug-like molecules. This suggests that bicyclic and monocyclic mimetics based on BH3 domains are much more efficient binding ligands than the longer peptides which they mimic.

Introduction

The ability of cells to undergo apoptosis is vital for the survival of an organism.[1] Bcl2 homology (BH) proteins regulate this pathway and are grouped into three sub-families. Pro-survival members Bcl-2, Bcl-xL, Bcl-w, Mcl-1, A1/BFL-1 maintain the survival signal within the cell. Pro-death affectors Bak and Bax directly trigger cell death. Finally, BH3-only members BID, BAD, BIM, BIK, EGl-1, BMF, PUMA, NOXA, BNIP3 and Beclin-1 indirectly promote cell death.[2] In the normal state, the network functions by pro-survival proteins sequestering and inhibiting pro-death function of Bak and Bax. When cellular or pathological signals indicate irreparable cellular damage, BH3-only members are produced to bind pro-survival proteins and displace Bak and Bax.[2] Released Bak/Bax then initiate apoptosis by oligomerising and inserting into the outer mitochondrial membrane leading to permeabilisation, cytochrome c release and eventually cell death.[2] Deregulation of this network occurs in cancer cells through the over-production of pro-survival proteins that ensure

Bak/Bax always remain sequestered even under cell damaging conditions that should trigger apoptosis. This promotes tumor growth by allowing diseased cells to either propagate[3] or release pro-inflammatory signals which protect the tumor from immune surveillance.[4] Evasion of apoptosis is a hallmark of cancer.[5]

Small molecules such as ABT-737,[6] helix-constrained stapled peptides[7–10] and foldamers[11] can mimic BH3-only members by binding to over-abundant pro-survival proteins, releasing Bak/Bax and reactivating apoptosis in cells. Crystal structures of BH3 peptides and small molecules bound to Bcl-xL and Bcl-2 exist (Fig. 1A, B). For peptides, 3–4 hydrophobic residues and a single acidic residue confer binding (Fig. 1B). One small molecule ABT-199 (Venetoclax®) has entered the clinic. There is intense interest in developing other small molecules, stapled peptides and foldamers to inhibit Bcl-2 proteins, reactivate apoptosis and treat cancer.

Previously developed stapled peptides mimicked the entire BH3 domains of BID, BIM and BAD (>20 residues).[7–10] Key binding residues are, however, contained within a shorter 10-residue segment (3 helical turns). These peptides were preorganised into an α-helix with a single hydrocarbon staple. Although substantially helical, peptidic regions flanking the staple suffer from low biological stability. Stapled BH3 peptides have equivalent activity to small molecules like ABT-737 but are 3–4 times higher in molecular weight. We previously developed a strategy to stabilise very short peptides (5-residues) in highly α-helical structures using K(i)–D($i+4$) lactam bridges.[12] We demonstrated that

[a] *Centre of Excellence in Advanced Imaging, Institute for Molecular Bioscience, The University of Queensland, Brisbane, Qld 4072, Australia. E-mail: d.fairlie@imb.uq.edu.au, n.shepherd@imb.uq.edu.au*

[b] *Structural Bioinformatics, BIOTEC, Technische Universität Dresden, Tatzberg 47–51, 01307 Dresden, Germany.*

[c] *Department of Biology and Biochemistry, University of Bath, Claverton Down, Bath BA2 7AY, United Kingdom.*

this staple conferred much higher α-helicity than alternatives.[13] Multiple such bridges incorporated in longer bioactive helical sequences allowed downsizing to just 'hotspot' binding regions. Removing unnecessary appendages improves biological stability.[14] Downsized versions of stapled BH3 peptides would also be easier and cheaper to produce. Their smaller molecular weight would make them more efficient binding ligands. Smaller molecules like ABT-737 (Fig. 1D) replicate the biological activity of entire BH3 domains whilst only mimicking ~8 residues. Thus, reported long stapled peptides should in principle be amenable to downsizing provided peptides are α-helical and correctly position key side-chains into complementary pockets on Bcl-xL. Here we describe efforts to downsize the BAD BH3 domain.

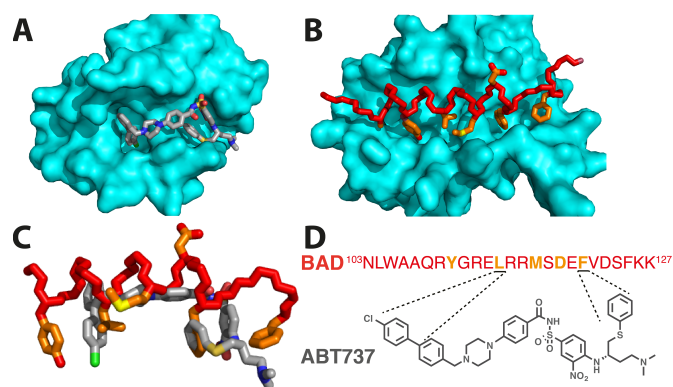**Fig. 1 A**) Crystal structure of ABT-737 (grey) bound to Bcl-xL (cyan) (pdb: 2yxj). **B**) Crystal structure of BAD(103–127) (red) bound to Bcl-xL (cyan) (pdb: 1g5j). **C**) Overlay of bound structures of ABT737 and BAD(103–127). **D**) Peptide sequence of BAD(103–127) and molecular structure of ABT-737. Key residues for binding shown in orange, those mimicked by ABT737 are indicated.

Results and discussion

Helix-stabilized and downsized versions of the BAD BH3 domain

We formulated three approaches to generate downsized and stapled versions of residues 103–127 in the BAD BH3 (hereafter, BAD 25-mer). Firstly, we made 19-, 12- and 8-residue peptides based on the central portion of the BAD 25-mer[15] containing a single K(i)-D($i+4$) lactam bridge (**5–7**). Secondly, we inserted two K(i)–D($i+4$) lactam bridges into the different fragments of the BAD 25-mer. These 12–14 residue BAD mimics (**8–11**) attempted to define a 'hotspot' within the sequence. Thirdly, we removed six residues from the N-terminus of the BAD 25-mer to give a 19-residue mimic with three helix inducing K(i)–D($i+4$) lactam constraints (**12**). Bridging positions were chosen based on crystal structures and prior SAR data. Generally these were positioned on the solvent exposed face of the helix. Linear peptides corresponding to each of these regions were also prepared (**1–4**). All peptide sequences are shown in Figure 2.

To determine the minimal functional region, we first investigated the 25-residue BAD BH3 domain and four truncated linear analogues (**1–4**, 13–19 residues; Fig. 2). We assessed structure by CD spectroscopy (Fig. 3A) and binding to Bcl-xL by fluores-

Fig. 2 BAD BH3 (103–127) and linear and cyclic peptides (**1–17**) synthesized in this study (Z = Norleucine, 1Nal = 1-Naphthylalanine, Aib = α-aminoisobutyric acid, 2Nal = 2-Naphthylalanine, F(Cl$_2$) = 3,4-dichlorophenylalanine). Underlined region indicates minimal region mimicked by ABT-737. All peptides were N-acetylated and C-amidated.

cence polarization (FP, Fig. 3B). The BAD 25-mer and shortened versions **1–4** all had little α-helical structure by CD spectroscopy (Fig. 3A). In the Bcl-xL binding assay the BAD 25-mer effectively competed with its fluorescently labeled derivative Flu-BAD (IC$_{50}$ 53 nM, Fig. 3B, red). Compounds **1–3** had IC$_{50}$ > 100 μM, while only the 19-residue **4** retained some binding (IC$_{50}$ 4.4 μM, Fig. 3B, orange).

K(i)–D($i+4$) lactam bridges induce high α-helicity into short unstructured peptides.[12–14] Therefore, a lactam constraint was inserted into peptide **4** in place of Arg8 and Glu12. These were equivalent positions occupied by the hydrocarbon staple used in previous studies.[7–10] This peptide (**5**) and two truncated versions (**6** and **7**) were all shorter than the BAD 25-mer by 5-, 12- and 19-residues, respectively. CD spectral fingerprints revealed a slight increase in α-helicity for **5** over the full length BAD 25-mer. The shorter **6** and **7** had 2–2.5-fold improved α-helicity (Fig. 4A). But peptides **5–7** all had weaker binding to Bcl-xL (Fig. 4B). The
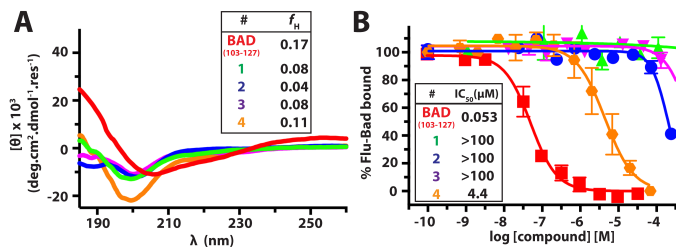
Fig. 3 A) CD spectra of BAD(103–127) and linear peptides **1–4**. **B)** Dose-response curves for synthetic compounds in a fluorescence polarization assay against Bcl-xL (error bars represent SEM, n ≥ 3). BAD(103–127) (–), **1** (–), **2** (–), **3** (–), **4** (–).

19-residue **5** was equipotent to its linear analogue **4** (IC$_{50}$ of 4.6 μM), while peptides **5** and **6** had IC$_{50}$ > 100 μM.
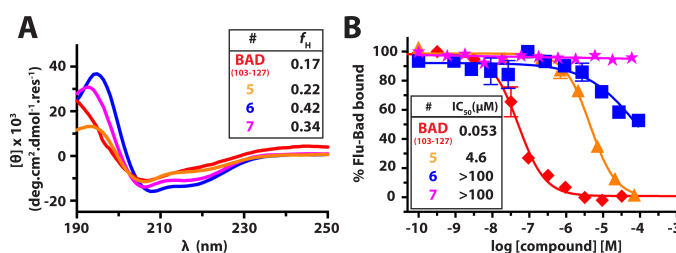

Fig. 4 A) CD spectra of BAD(103–127) and monocyclic peptides **5–7**. **B)** Dose-response curves for synthetic compounds in a fluorescence polarization assay against Bcl-xL (error bars represent SEM, n ≥ 3). BAD(103-127) (–), **5** (–), **6** (–), **7** (–).

Next, we incorporated two or three lactam bridges into 12–19 residue segments that spanned the entire BAD 25-mer (peptides **8–12**). Introducing a second and third bridge peptides led to substantially improved α-helicity over linear sequences as judged by CD spectra (2.6–6.2-fold, Fig. 5A). However, improved α-helicity in these smaller peptides did not translate to improved binding over the BAD 25-mer (Fig. 5B). Tricyclic **12** was the most potent (IC$_{50}$ 252 nM) followed by the bicyclic **9** (IC$_{50}$ 1.5 μM) and **11** (IC$_{50}$ 40 μM). These results indicate the central portion of the BAD BH3 helix (**9**) provides most of the binding energy. The constrained C-terminal region (**11**) contributes a small amount to binding. The N-terminal region (**8**) appears less important for binding. The positioning of lactam bridges was critical. The back-to-back staple arrangement in **10** abolished activity, likely due to steric clashes.
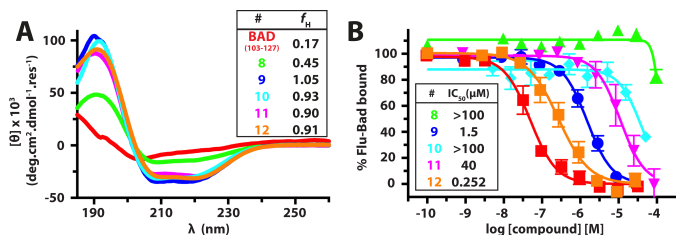

Fig. 5 A) CD spectra of BAD(103–127) and bicyclic peptides **8–11** and tricycle **12**. **B)** Dose-response curves for synthetic compounds in a fluorescence polarization assay against Bcl-xL (error bars represent SEM, n ≥ 3). BAD(103-127) (–), **8** (–), **9** (–), **10** (–), **11** (–), **12** (–).

These data suggested that α-helicity was less important contributor to inhibitor potency than peptide length. To probe this relationship we compared helicity and activity across related peptides **4**, **5**, and **12**; **2**, **6**, and **9**; and, **3** and **11**. Helicity improved inhibitory potency by 1–2 log units (Fig. 6). However, increasing α-helicity did not compensate for loss of interacting sidechains through downsizing. Bcl-xL appears to lack a defined 'hot-spot'. Interactions across the N-, central and C-terminal portions of the BAD BH3 together provide high affinity.
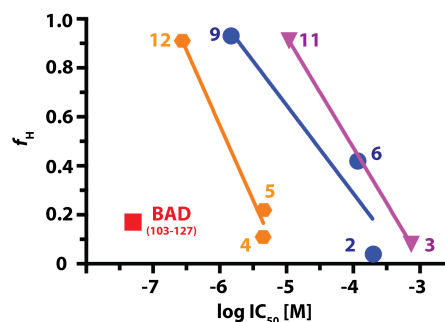

Fig. 6 Relationship between fractional helicity and inhibitory potency for linear and cyclic mimetics of the BAD-BH3 domain.

The activity of **9** (IC$_{50}$ 1.5 μM) was lower than for the BAD 25-mer, ABT-737 or reported compound SAH-BID.[8] But we had removed 11 residues from the BAD 25-mer and yet still retained activity. Thus, we decided to compare the efficiency of our downsized ligands. We calculated the binding efficiency index[16] (BEI) to determine whether downsizing was worthwhile. Table 1 shows the BEI of bicyclic **9** (3.55) was better than the BAD BH3 (2.32) and SAH-BID (2.71) but worse than ABT-737 (9.23). We reasoned if **9** could be optimised to an IC$_{50}$ to 40 nM without much increase in molecular weight, the BEI would be 4.6. This is only 2-fold better than the BAD-25-mer, and still 2-fold worse than ABT-737. Thus, it seemed prudent to find an even smaller lead with a BEI closer to ABT-737.

Table 1 Comparison of compound binding efficiency indices (BEI) for Bcl-xL

Compound	MW	pIC$_{50}$	BEI*
BAD BH3	3134	7.3	2.32
5	2510	5.3	2.11
9	1633	5.8	3.55
12	2305	6.6	2.86
15	956	5.2	5.44
16	1043	5.2	4.99
17	1063	5.2	4.89
SAH-BID[8]	2726	7.4	2.71
ABT-737[6]	813	7.5	9.23

* Binding Efficiency Index (BEI) = pIC$_{50}$ / MW (in kDa)

Monocycle library

ABT-737 mimics three side chains of the BAD BH3 domain: Leu114, Met117 and Phe121. Therefore, we decided to prepare monocyclic octapeptides spanning the Leu114–Phe121 region. We prepared a small library of 26 compounds using macrocyclic

octapeptide **7** as a scaffold. (Fig. 7A). Leu1 and Nle4 in **7** were substituted with Phe or 1-Naphthylalanine (1Nal). Phe8 in **7** was substituted with Nle or homophenylalanine (hPhe). Although **7** was essentially inactive, we hypothesized that incorporating aromatic groups to better resemble ABT-737 might improve activity. Each compound was screened at 10 μM in the FP assay. Of these compounds, 25 displaced less than 20% Flu-BAD. One compound (**13**, IC$_{50}$ 7.9 μM) displaced 25% Flu-BAD BH3 and differed from **7** only in its first residue, 1Nal instead of Leu. The acyclic analogue Ac-1Nal-RR-Nle-ADDF-NH$_2$ (**14**) had IC$_{50}$ 36 μM (Fig 7B), highlighting the importance of helix stabilization.

Fig. 7 A) Cyclic peptide library based on the BAD(114–121) region (1Nal = 1-Naphthylalanine, hPhe = Homophenylalanine). Single concentration triplicate screen of the ability cyclic peptides [10 μM] to displace fluorescein-labelled BAD(103–127) from Bcl-xL. **B)** Dose response curves for BAD(103–127) (−), Ac-1NalR[KNleADD]F-NH$_2$ (**13**, −), and Ac-1NalRRADDF-NH$_2$ (**14**, −) in a fluorescence polarization assay against Bcl-xL (error bars represent SEM, n ≥ 3).

Next we attempted to improve the activity of **13**. We replaced Arg2 with Aib to increase helicity within the N-terminal exocyclic portion (**15**, Fig. 8, IC$_{50}$ 6.3 μM). We made N-terminal substitutions with non-peptidic capping groups (1-naphthylpropanoyl, 1-naphthylpropenoyl, 1-naphthyloxyacetyl) or C-terminal substitutions with unnatural aromatic amino acids (3,4-dichlorophenylalanine, Phe(Cl$_2$); serine-O-benzyl ester, Ser(OBn); and 2-Naphthylalanine, 2Nal). All N-terminal substitutions were less active, whilst Phe(Cl$_2$) (**16**) and 2Nal (**17**) at the C-terminus offered no improvement (IC$_{50}$ 5.8 and 7.0 μM, Fig. 8).

The new leads **15–17** were now one third of the size of the BAD 25-mer and SAH-BID. Despite having low micromolar activity, they are more efficient ligands (BEI 4.89–5.44, Table 1). Monocycles must still be optimised to equipotency with ABT-737 and SAH-BID. If achieved whilst maintaining their current molecular weight (1000 Da), their BEI would be much more favourable (~7.5). To show further potential of bicyclic **9** and monocyclic **15–17** as inhibitors of Bcl-xL/2 function, we evaluated leukemic T-cell (Jurkat E6.1) killing abilities of **9** and **16** using an MTT assay. The linear BAD 25-mer showed weak activity (IC$_{50}$ 60 μM), whilst **9** and **16** both showed improved cell killing ability with IC$_{50}$ 40 and 18 μM, respectively (Fig. 9). Thus, the BAD 25-mer can be downsized to smaller cyclic peptides with appreciable binding to Bcl-xL and activity in cells.
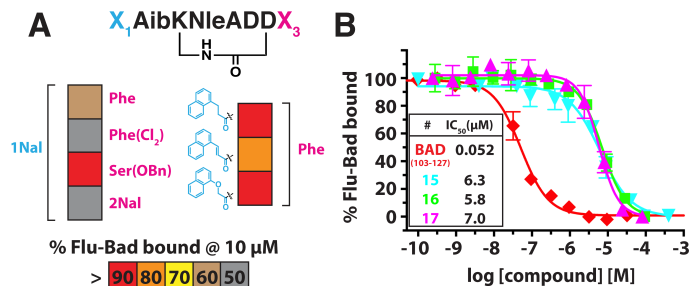

Fig. 8 A) Cyclic peptide library based on the BAD(114–121) region (Phe(Cl$_2$) = 3,4-Dichlorophenylalanine, Ser(OBn) = Serine-O-benzyl ester, 2Nal = 2-Naphthylalanine). Single concentration triplicate screen of the ability cyclic peptides [10 μM] to displace fluorescein-labelled BAD(103–127) from Bcl-xL. **B)** Dose response curves for BAD(103–127) (−), Ac-1NalAib[KNleADD]F-NH$_2$ (**15**, −), Ac-1NalAib[KNleADD]F(Cl$_2$)-NH$_2$ (**16**, −), Ac-1NalAib[KNleADD]2Nal-NH$_2$ (**17**, −)(error bars represent SEM, n ≥ 3).
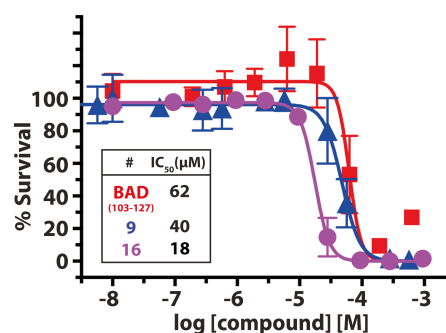

Fig. 9 Dose-response curves of compounds in an MTT assay against Jurkat E6.1 cells (error bars represent SEM, n ≥ 3). BAD BH3 (103–127) (−), bicyclic **9** (−), and monocyclic **16** (−).

Conclusion

Forty-five helix-stabilized and downsized analogues of the BAD BH3 domain were structurally characterized by CD spectroscopy and their *in vitro* inhibition of Bcl-xL was examined. Using one to three K(i)–D(i+4) lactam bridges to constrain different regions of the BAD BH3 domain, we have shown: i) the central portion (residues 108–121) is the critical region for BAD BH3 activity; ii) α-helicity is important for binding to Bcl-xL, conferring a 1–2 log unit improvement in IC$_{50}$; iii) the BAD BH3 can be downsized to bicyclic and monocyclic mimics with low micromolar affinity for Bcl-xL (e.g. **9**, IC$_{50}$ 1.5 μM; **15–17**, IC$_{50}$ 5.8–7 μM). Subtle differences in helicity or the helix constraint might contribute to lower Bcl-xL affinity compared to SAH-BID[8] and SAH-BIM.[9] However, the clear difference is the much smaller size of **9** (13-residues), **13**, **15–17** (8-residues) relative to SAH-BID (23-residues) and SAH-BIM (21-residues). Additional interactions with Bcl-xL likely account for higher affinity for the longer peptides. Despite reduced activity, these downsized molecules are actually more efficient ligands. Their binding efficiency indices are closer to ABT-737 than full length BAD BH3 or stapled peptides such as SAH-BID. Compounds **9** and **16** showed higher cell killing potency than the BAD 25-mer. Overall bicyclic and monocyclic BH3 mimetics identified here are promising candidates for optimisation as Bcl2-protein inhibitors. These studies further demonstrate the utility of

K(i)–D(i+4) lactam bridges for helix pre-organisation. Our work provides a platform for investigating protein-protein interactions and developing small, efficient peptidomimetic inhibitors.

Experimental

General

Fmoc-amino acids were purchased from Novabiochem (Melbourne, Australia) and Chemimpex (USA). O-Benzotriazole-N,N,N',N'-tetramethyluronium-hexafluorophosphate (HBTU) was obtained from IRIS Biotech GmbH (Marktredwitz, Germany) and Chemimpex (USA). HCTU was purchased from Chemimpex (USA). HATU was purchased from Chemimpex (USA). All other reagents were of peptide synthesis grade and obtained from Auspep (Melbourne, Australia).

Molecular modelling

Crystal structures were visualised using MacPymol.[17] The PISA server[18] was used to assist characterising protein-protein interactions.

Peptide synthesis and purification

Peptides were synthesized manually by standard solid phase methods using HBTU/DIPEA activation of Fmoc on Rink Amide resins (substitution 0.3–0.5 mmol/g, 0.2–0.5 mmol scale). 4 equiv of Fmoc-protected amino acid, 4 equiv of HBTU and 4 equiv of DIPEA were used in each coupling. Fmoc deprotection involved 2×3 min treatments with excess piperidine/DMF (1:1). Coupling yields were monitored by quantitative ninhydrin assay. Arginine residues were double coupled to prevent deletions within the sequence. After the final (N-terminal) residue was coupled, the compound was acetyl capped with 2 equiv acetic acid, 2 equiv HBTU and 2 equiv DIPEA respectively. For cyclic peptides the phenylisopropyl ester of aspartic acid and methyltrityl group of lysine were removed by treating the peptide resin with 3% TFA, 2.5% TIPS in DCM (5×2 min). The resin was neutralised by washing with 5% DIPEA in DMF (2×3 min). Cyclization was affected on-resin using BOP, DIPEA in DMF. Fluorescein-labelled BAD (Flu-BAD) was synthesised as above omitting the cyclisation and capping procedures. After the final glutamine was coupled the peptide was deprotected and Fmoc-6-aminohexanoic acid (AHA) was coupled analogously to other amino acids. Following subsequent Fmoc-deprotection, four molar equivalents of 5(6)-carboxyfluorescein and DIC were coupled overnight. After synthesis the peptide resins were washed with DMF, MeOH/DCM and DCM, dried under nitrogen with suction for 20 min. Peptides were cleaved using 95% TFA, 2.5% TIPS, 2.5% H$_2$O. Peptides were precipitated with diethyl ether and then decanted to give white solids that were re-dissolved in 1:1 acetonitrile/water and lyophilised. The crude peptides were purified by rp-HPLC (Vydac C18 column, 300 Å 22×250 mm, 214 nm, Solvent A=0.1% TFA in H$_2$O, Solvent B=0.1% TFA, 10% H$_2$O in acetonitrile. Gradient: 0% B to 70% B over 35 min). Peptides were characterised by analytical rp-HPLC and ESI-MS and in all cases were >92% pure.

Circular dichroism

CD experiments were performed on a Jasco Model J-710 spectropolarimeter routinely calibrated with (1S)-(+)-10-camphorsulfonic acid. Spectra were recorded in a 0.1 cm Jasco cell between 260 and 185 nm at 50 nm/min with a bandwidth of 1.0 nm, response time of 2 s, resolution step width of 0.1 nm, and sensitivity of 20, 50, or 100 mdeg. Each spectrum represents the average of five scans with smoothing to reduce noise. Peptide samples for CD spectroscopy were dissolved in 18 MΩ distilled water (~3-4 mg/mL). 500 μL of each stock solution was then diluted 1:1 with phosphate buffer pH 7.4. Solutions were then prepared for each sample with final concentrations ranging from 50 to 800 μM in 10 mM sodium phosphate buffer (pH 7.4). Over this concentration range the CD intensity was found to be independent of concentration ruling out aggregation as a stabilizing effect. The remaining 500 μL from the initial stock solution was used for accurate concentration determination. Accurate concentrations of stock solutions were determined by 1D 1H NMR spectroscopy based on integrations of non-exchangeable proton signals using the PULCON method.[19] Briefly 475 μL of the initial peptide stock solution was mixed with 50 μL of D$_2$O and spiked with an internal standard, 25 μL of 10.077 mM DSS. 1D ^{1}H NMR spectra were then recorded with gradient water suppression and a relaxation delay (d1) of 30 s to allow for full relaxation of peptide and DSS ^{1}H signals to facilitate accurate integration of proton signals with S/N > 250:1. Fractional helicity was calculated using the equation derived by Luo $et.$ $al.$[20]

Fluorescence polarisation assay

Assays were conducted as previously described.[21] Briefly, the assay buffer contained 20 mM phosphate buffer, 50 mM NaCl, 1 mM EDTA and 0.05% pluronic F-127 (Invitrogen, CA, USA) and the fluorescent probe Flu-BAD (fluorescein-AHA-NLWAAQRYGRELRRNleSDEFFVDSFKK-NH$_2$, AHA = 6-aminohexanoic acid). The equilibrium binding experiments of the fluorescein-labelled BAD peptide to Bcl-xL (R&D Systems) was determined in a 96-well assay plate contained 15 nM fluorescent peptide, and increasing concentrations of protein in assay buffer in a final volume of 200 μL. The plate was incubated for 20 min and then measured using Envision plate reader (Perkin Elmer) at room temperature with an excitation wavelength of 480 nm and an emission wavelength of 535 nm. Millipolarisation units (mP) were calculated using the equation below by the Envision software:

$$mP = \frac{S - (G \times P)}{(S - (G \times P)) \times 1000}$$

where S and P are background subtracted fluorescence rates and G is an instrument and assay dependent factor (determined for each plate). K$_d$ values were calculated by fitting data to a sigmoidal dose-response nonlinear regression model (equation below) using GraphPad Prism (GraphPad Software Inc., San Diego, CA). The competition studies were performed in a 96-well plate containing 15 nM fluorescein-labelled BAD, 10 nM Bcl-xL and increasing concentrations of test compounds in assay buffer, in a final volume of 200 μL. The plate was incubated at room temper-

ature for 20 min and then measured as described above. The IC_{50}, or the concentration at which 50% of bound peptide is displaced, was obtained by fitting the data to a sigmoidal dose-response nonlinear regression model (Prism5, GraphPad Software):

$$Y = \frac{bottom(top - bottom)}{1 + 10^{(logEC_{50} - X) \times hillslope}}$$

Cell culture

The human leukaemia T cell line (Jurkat E6.1 cells) were cultured in GIBCO® RPMI (Invitrogen, CA, USA) medium supplemented with 10% FBS (Invitrogen, CA, USA), GIBCO® Pen/Strep (50 units/mL penicillin and 50 μg/ml streptomycin, Invitrogen, CA, USA), GIBCO® NEAA (non-essential amino acids; 1×, Invitrogen, CA, USA) and GIBCO® L-glutamic acid (final concentration 2 mM, Invitrogen, CA, USA). Cells were grown to 80-90% confluency at 37 °C (5% CO_2) and were passaged at a ratio of 1:10 every three to four days.

Cytotoxicity assay

To assess the cytotoxicity of peptides on Jurkat E6.1 cells, we used the standard MTT assay. In this assay, the yellow tetrazolium salt MTT (3-(4,5-dimethylthiazol-2-yl)-2,5-diphenyltetrazolium bromide) can be reduced to a purple formazan product in the mitochondria of metabolically active cells. We were able to quantify the formation of blue formazan at 570 nm, relating absorbance to the number of viable cells. We expected that the peptides would have different stability in serum so to minimise this effect, the MTT assays were conducted in serum-free media. Jurkat T cells were washed three times in serum-free media and subsequently plated into a clear, flat-bottom, 96-well microtitre plate at 5×10^4 cells/well. Cells were then treated with 10 μL of peptide at various concentrations. The microtitre plate was then incubated for 48 hours at 37 °C (5% CO_2). MTT (Sigma-Aldrich, NY, USA) was added to each well (10 μL, final concentration 50 μg/mL). The treated plate was incubated in the dark for two hours at 37 °C (5% CO_2). 10% SDS in water/isopropanol (1:1) was added (100 μL per well) and incubated at 37 °C overnight, to allow complete solubilisation of the purple formazan product. Absorbance was read at 570 nm, with background subtraction 630–690 nm, on BioTekPowerWave XS micro-well plate reader. A dose-response curve was obtained by fitting data to a sigmoidal dose-response nonlinear regression model (Prism5, GraphPad Software).

Acknowledgments

References

1 S. Elmore, *Toxicol. Pathol.*, 2007, **35**, 495–516.

2 P. E. Czabotar, G. Lessene, A. Strasser and J. M. Adams, *Nat. Rev. Mol. Cell. Biol.*, 2014, **15**, 49–63.

3 J. M. Brown and L. D. Attardi, *Nat. Rev. Cancer*, 2005, **5**, 231–237.

4 S. I. Grivennikov, F. R. Greten and M. Karin, *Cell*, 2010, **140**, 883–899.

5 D. Hanahan and R. A. Weinberg, *Cell*, 2011, **144**, 646–674.

6 T. Oltersdorf, S. W. Elmore, A. R. Shoemaker, R. C. Armstrong, D. J. Augeri, B. A. Belli, M. Bruncko, T. L. Deckwerth, J. Dinges, P. J. Hajduk, M. K. Joseph, S. Kitada, S. J. Korsmeyer, A. R. Kunzer, A. Letai, C. Li, M. J. Mitten, D. G. Nettesheim, S. Ng, P. M. Nimmer, J. M. O'Connor, A. Oleksijew, A. M. Petros, J. C. Reed, W. Shen, S. K. Tahir, C. B. Thompson, K. J. Tomaselli, B. Wang, M. D. Wendt, H. Zhang, S. W. Fesik and S. H. Rosenberg, *Nature*, 2005, **435**, 677–681.

7 R. Rezaei Araghi, J. A. Ryan, A. Letai and A. E. Keating, *ACS Chem. Biol.*, 2016, **11**, 1238–1244.

8 L. D. Walensky, A. L. Kung, I. Escher, T. J. Malia, S. Barbuto, R. D. Wright, G. Wagner, G. L. Verdine and S. J. Korsmeyer, *Science*, 2004, **305**, 1466–1470.

9 L. D. Walensky, K. Pitter, J. Morash, K. J. Oh, S. Barbuto, J. Fisher, E. Smith, G. L. Verdine and S. J. Korsmeyer, *Mol. Cell*, 2006, **24**, 199–210.

10 M. L. Stewart, E. Fire, A. E. Keating and L. D. Walensky, *Nat. Chem. Biol.*, 2010, **6**, 595–601.

11 J. W. Checco, E. F. Lee, M. Evangelista, N. J. Sleebs, K. Rogers, A. Pettikiriarachchi, N. J. Kershaw, G. A. Eddinger, D. G. Belair, J. L. Wilson, C. H. Eller, R. T. Raines, W. L. Murphy, B. J. Smith, S. H. Gellman and W. D. Fairlie, *J. Am. Chem. Soc.*, 2015, **137**, 11365–11375.

12 N. E. Shepherd, H. N. Hoang, G. Abbenante and D. P. Fairlie, *J. Am. Chem. Soc.*, 2005, **127**, 2974–2983.

13 A. D. de Araujo, H. N. Hoang, W. M. Kok, F. Diness, P. Gupta, T. A. Hill, R. W. Driver, D. A. Price, S. Liras and D. P. Fairlie, *Angew. Chem. Int. Ed. Engl.*, 2014, **53**, 6965–6969.

14 R. S. Harrison, N. E. Shepherd, H. N. Hoang, G. Ruiz-Gomez, T. A. Hill, R. W. Driver, V. S. Desai, P. R. Young, G. Abbenante and D. P. Fairlie, *Proc. Natl. Acad. Sci. U.S.A.*, 2010, **107**, 11686–11691.

15 A. M. Petros, D. G. Nettesheim, Y. Wang, E. T. Olejniczak, R. P. Meadows, J. Mack, K. Swift, E. D. Matayoshi, H. Zhang, C. B. Thompson and S. W. Fesik, *Protein Sci.*, 2000, **9**, 2528–2534.

16 C. Abad-Zapatero and J. T. Metz, *Drug. Discov. Today*, 2005, **10**, 464–469.

17 *The PyMol Molecular Graphics System*, 2015.

18 E. Krissinel and K. Henrick, *J. Mol. Biol.*, 2007, **372**, 774–797.

19 G. Wider and L. Dreier, *J. Am. Chem. Soc.*, 2006, **128**, 2571–2576.

20 P. Luo and R. L. Baldwin, *Biochemistry*, 1997, **36**, 8413–8421.

21 H. Zhang, P. Nimmer, S. H. Rosenberg, S. C. Ng and M. Joseph, *Anal. Biochem.*, 2002, **307**, 70–75.
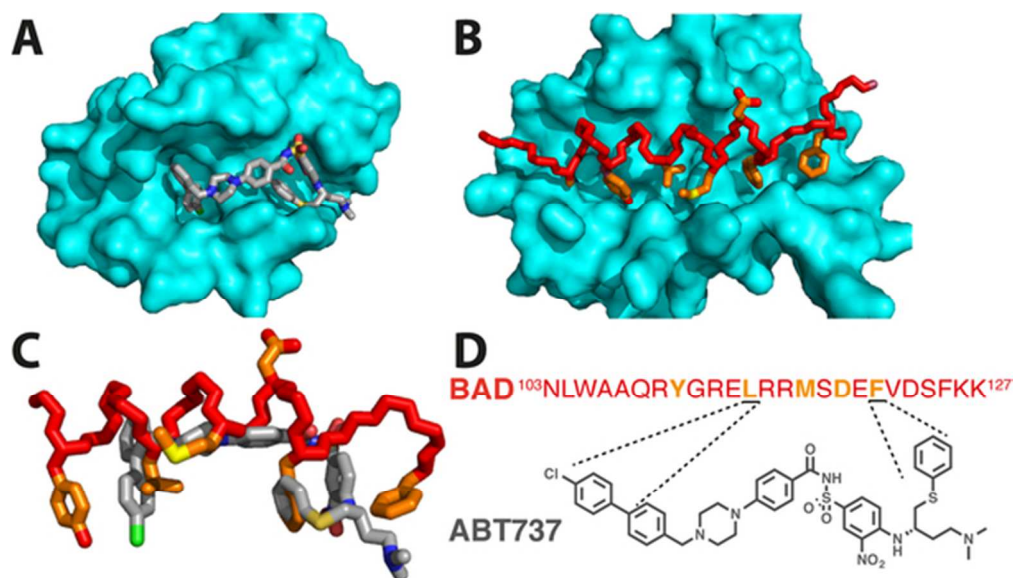
A) Crystal structure of ABT-737 (grey) bound to Bcl-xL (cyan) (pdb: 2yxj). B) Crystal structure of BAD(103-127) (red) bound to Bcl-xL (cyan) (pdb: 1g5j). C) Overlay of bound structures of ABT737 and BAD(103-127). D) Peptide sequence of BAD(103-127) and molecular structure of ABT-737. Key residues for binding shown in orange, those mimicked by ABT737 are indicated.
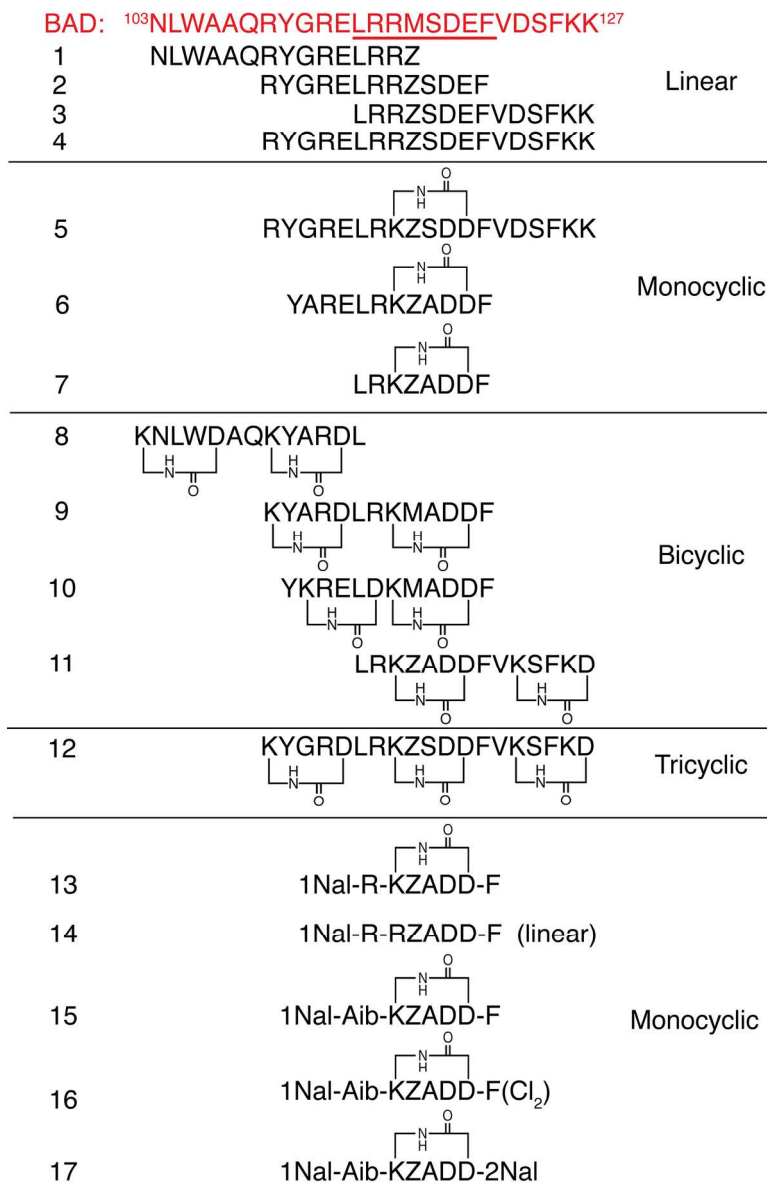
51x29mm (300 x 300 DPI)

Fig. 2 BAD BH3 (103–127) and linear and cyclic peptides (1–17) synthesized in this study (Z = Norleucine, 1Nal = 1-Naphthylalanine, Aib = alpha-aminoisobutyric acid, 2Nal = 2-Naphthylalanine, F(Cl2) = 3,4-dichlorophenylalanine). Underlined region indicates minimal region mimicked by ABT-737. All peptides were N-acetylated and C-amidated.
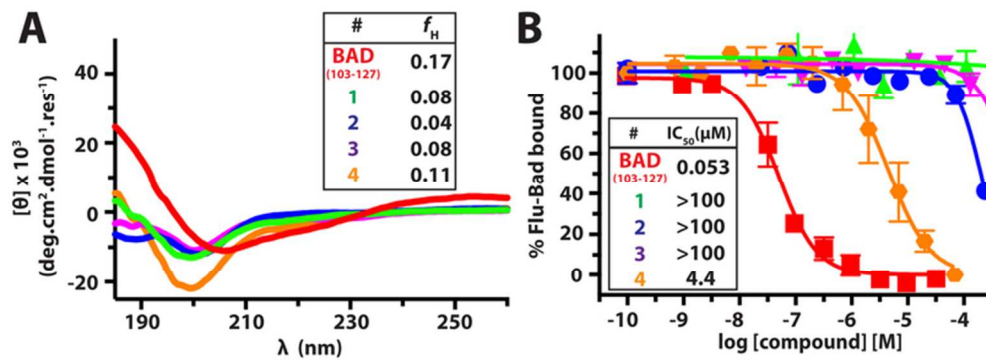
140x219mm (300 x 300 DPI)

Fig. 3 A) CD spectra of BAD(103–127) and linear peptides 1–4. B) Dose-response curves for synthetic compounds in a fluorescence polarization assay against Bcl-xL (error bars represent SEM, n > 3). BAD(103–127) (red), 1 (green), 2 (blue), 3 (magenta), 4 (orange).
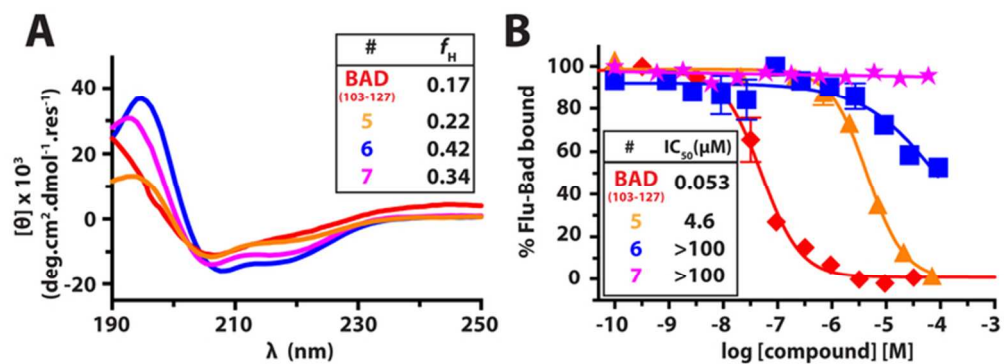
69x24mm (300 x 300 DPI)

Fig. 4 A) CD spectra of BAD(103–127) and monocyclic peptides 5–7. B) Dose-response curves for synthetic compounds in a fluorescence polarization assay against Bcl-xL (error bars represent SEM, n > 3). BAD(103-127) (red), 5 (orange), 6 (blue), 7 (magenta).
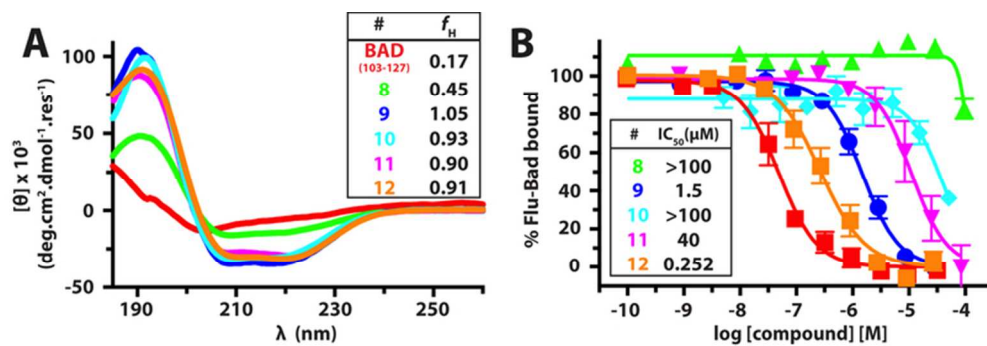
66x23mm (300 x 300 DPI)

Fig. 5 A) CD spectra of BAD(103–127) and bicyclic peptides 8–11 and tricycle 12. B) Dose-response curves for synthetic compounds in a fluorescence polarization assay against Bcl-xL (error bars represent SEM, n > 3). BAD(103–127) (red), 8 (green), 9 (blue), 10 (cyan), 11 (magenta), 12 (orange).
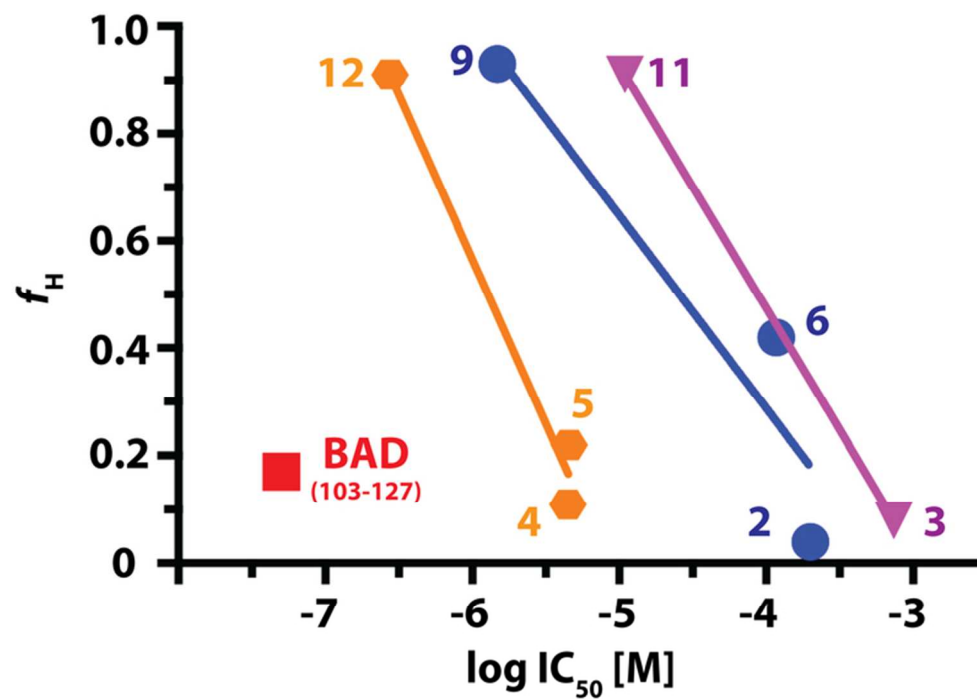
68x22mm (300 x 300 DPI)

Fig. 6 Relationship between fractional helicity and inhibitory potency for linear and cyclic mimetics of the BAD-BH3 domain.
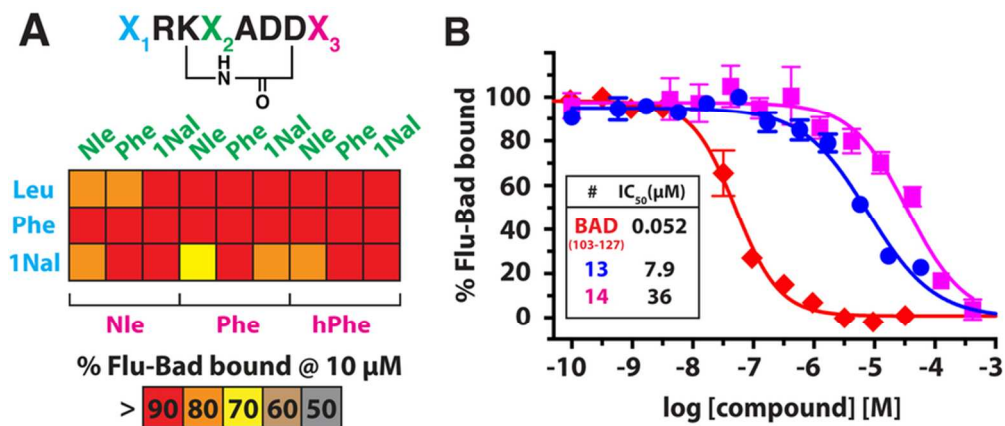
69x50mm (300 x 300 DPI)

Fig. 7 A) Cyclic peptide library based on the BAD(114–121) region (1Nal = 1-Naphthylalanine, hPhe = Homophenylalanine). Single concentration triplicate screen of the ability cyclic peptides [10 mM] to displace fluorescein-labelled BAD(103–127) from Bcl-xL. B) Dose response curves for BAD(103–127) (red), Ac-1NalR[KNleADD]F-NH2 (13, blue), and Ac-1NalRRADDF-NH2 (14, magenta) in a fluorescence polarization assay against Bcl-xL (error bars represent SEM, n > 3).
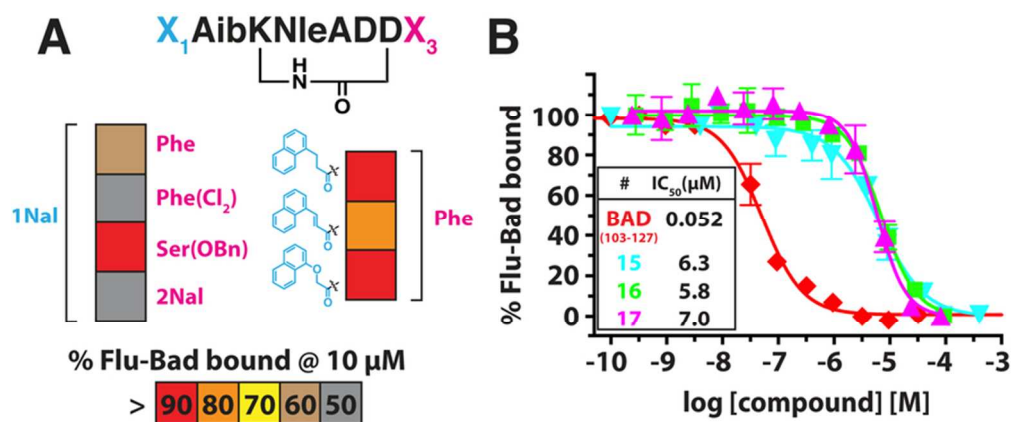
78x33mm (300 x 300 DPI)

Fig. 8 A) Cyclic peptide library based on the BAD(114–121) region (Phe(Cl2) = 3,4-Dichlorophenylalanine, Ser(OBn) = Serine-O-benzyl ester, 2Nal = 2-Naphthylalanine). Single concentration triplicate screen of the ability cyclic peptides [10 mM] to displace fluorescein-labelled BAD(103–127) from Bcl-xL. B) Dose response curves for BAD(103–127) (red), Ac-1NalAib[KNleADD]F-NH2 (15, cyan), Ac-1NalAib[KNleADD]F(Cl2)-NH2 (16, green), Ac-1NalAib[KNleADD]2Nal-NH2 (17, magenta) (error bars represent SEM, n > 3).

75x31mm (300 x 300 DPI)

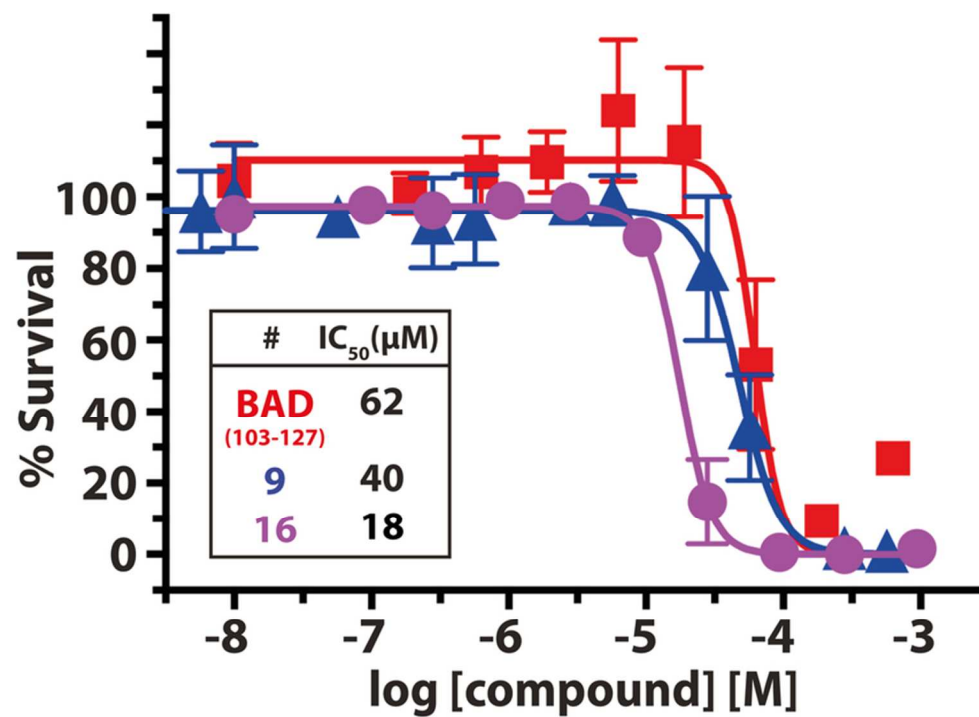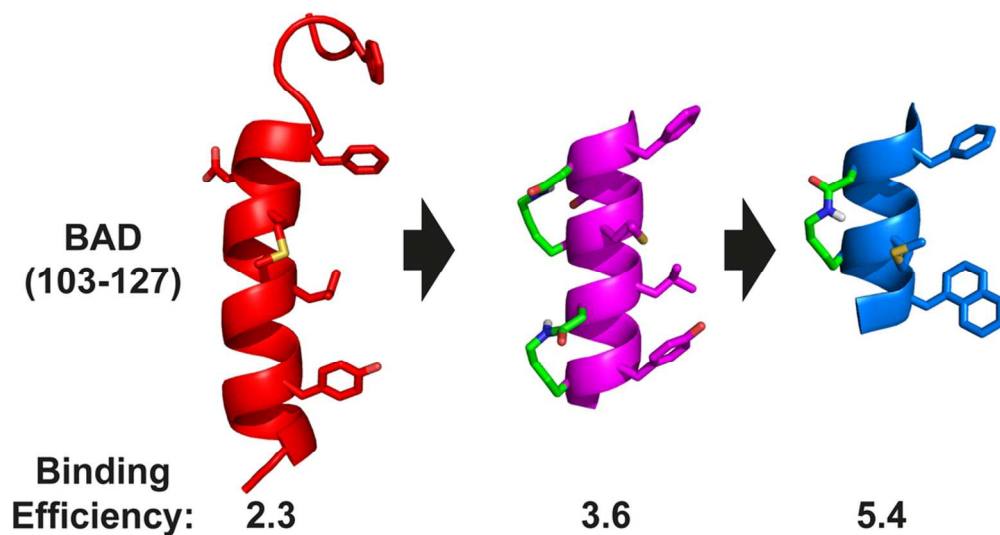Fig. 9 Dose-response curves of compounds in an MTT assay against Jurkat E6.1 cells (error bars represent SEM, n > 3). BAD BH3 (103–127) (red), bicyclic 9 (blue), and monocyclic 16 (purple).

73x52mm (300 x 300 DPI)

BAD
(103-127)

Binding
Efficiency: 2.3   3.6   5.4

TOC Entry: The BAD BH3 domain was downsized into small efficient macrocycles with affinity for Bcl-xL.

94x51mm (300 x 300 DPI)

Supplementary data

Downsizing the BAD BH3 peptide to small constrained α-helices with improved ligand efficiency

Nicholas E Shepherd,[a*] Rosemary S Harrison,[a] Gloria Ruiz-Gomez,[a,b] Giovanni Abbenante,[a] Jody M. Mason[c] and David P. Fairlie[a*]

[a]*Institute for Molecular Bioscience, The University of Queensland, Brisbane, Qld 4072, Australia*
[b]*Structural Bioinformatics, BIOTEC, Technische Universität Dresden, Tatzberg 47-51, 01307 Dresden, Germany.*
[c]*Department of Biology and Biochemistry, University of Bath, Claverton Down, Bath BA2 7AY, United Kingdom*

*Corresponding authors: d.fairlie@imb.uq.edu.au, n.shepherd@imb.uq.edu.au

Table 1. Compound characterisation data

#	Sequence	$[M+H]^+$ Calc.	$[M+H]^+$ Found	HPLC R_t
BAD-BH3	Ac-NLWAAQRYGRELRRMSDEFVDSFKK-NH$_2$	3142.59	3142.97	14.67
Flu-BAD	Flu-AHA-NLWAAQRYGRELRRMSDEFVDSFKK- NH$_2$	3571.05	3571.34	14.34
1	Ac-NLWAAQRYGRELRR*Nle*-NH$_2$	1943.25	1943.11	14.17
2	Ac-QRYGRELRR*Nle*SDEF-NH$_2$	1866.08	1866.67	14.68
3	Ac-LRR*Nle*SDEFVDSFKK-NH$_2$	1781.05	1780.59	14.53
4	Ac-QRYGRELRR*Nle*SDEFVDSFKK-NH$_2$	2570.90	2570.55	14.25
5	Ac-QRYGRELR[K*Nle*SDD]FVDSFKK-NH$_2$-	2510.85	2510.32	14.58
6	Ac-YARELR[K*Nle*ADD]F-NH$_2$	1518.79	1518.64	14.75
7	Ac-LR[K*Nle*ADD]F-NH$_2$	999.04	999.55	15.33
8	Ac-[KNLWD]AQ[KYARD]L-NH$_2$	1625.86	1625.21	15.04
9	Ac-[KYARD]LR[KMADD]F-NH$_2$	1632.89	1632.44	15.22
10	Ac-Y[KRELD][KMADD]F-NH$_2$	1534.72	1535.26	15.81
11	Ac-LR[K*Nle*ADD]FV[KSFKD]-NH$_2$	1685.93	1686.03	15.38
12	Ac-[KYGRD]LR[KNleSDD]FV[KSFKD]-NH$_2$	2304.64	2305.28	15.29
13	Ac-*1Nal*R[K*Nle*ADD]F-NH$_2$	1083.55	1083.53	15.74
14	Ac-*1Nal*RR*Nle*ADEF-NH$_2$	1143.58	1143.89	14.74
15	Ac-*1Nal Aib*[K*Nle*ADD]F-NH$_2$	955.48	955.66	16.31
16	Ac-*1Nal Aib*[K*Nle*ADD]*Phe(Cl$_2$)*-NH$_2$	1042.88	1042.51	16.02
17	Ac-*1Nal Aib*[K*Nle*ADD]*2Nal*-NH$_2$	1062.52	1063.34	16.35
18	Ac-LR[K*Nle*ADD]*hPhe*-NH$_2$	1013.57	1012.97	15.24
19	Ac-LR[KFADD]*hPhe*-NH$_2$	1047.55	1046.86	15.55
20	Ac-LR[K*1Nal*ADD]*hPhe*-NH$_2$	1047.55	1046.86	15.24

21	Ac-FR[K*Nle*ADD]*hPhe*-NH$_2$	1047.55	1047.59	15.56
22	Ac-FR[KFADD]*hPhe*-NH$_2$	1081.53	1081.49	15.55
23	Ac-FR[K*1Nal*ADD]*hPhe*-NH$_2$	1131.55	1131.40	16.11
24	Ac-*1Nal*R[K*Nle*ADD]*hPhe*-NH$_2$	1097.51	1097.57	16.16
25	Ac-*1Nal*R[KFADD]*hPhe*-NH$_2$	1131.45	1131.55	16.11
26	Ac-*1Nal*R[K*1Nal*ADD]*hPhe*-NH$_2$	1181.38	1181.56	16.74
27	Ac-LR[KFADD]F-NH$_2$	1033.53	1032.91	15.18
28	Ac-LR[K*1Nal*ADD]F-NH$_2$	1083.55	1082.84	15.89
29	Ac-FR[K*Nle*ADD]F-NH$_2$	1033.53	1033.65	15.23
30	Ac-FR[KFADD]F-NH$_2$	1067.61	1067.52	15.24
31	Ac-FR[K*1Nal*ADD]F-NH$_2$	1117.53	1117.41	15.77
32	Ac-*1Nal*R[KFADD]F-NH$_2$	1117.53	1117.51	15.65
33	Ac-*1Nal*R[K*1Nal*ADD]F-NH$_2$	1167.55	1167.33	16.19
34	Ac-LR[K*Nle*ADD]*Nle*-NH$_2$	965.57	965.81	15.21
35	Ac-LR[KFADD]*Nle* -NH$_2$	999.55	999.72	15.01
36	Ac-LR[K*1Nal*ADD]*Nle* -NH$_2$	1049.57	1049.65	15.80
37	Ac-FR[K*Nle*ADD]*Nle* -NH$_2$	999.55	999.66	15.17
38	Ac-FR[KFADD]*Nle* -NH$_2$	1033.53	1033.61	14.98
39	Ac-FR[K*1Nal*ADD]*Nle* -NH$_2$	1083.55	1083.51	15.56
40	Ac-*1Nal*R[K*Nle*ADD]*Nle* -NH$_2$	1049.57	1049.38	16.67
41	Ac-*1Nal*R[KFADD]*Nle* -NH$_2$	1083.55	1083.66	15.61
42	Ac-*1Nal*R[K*1Nal*ADD]*Nle* -NH$_2$	1133.22	1133.57	16.24
43	Ac-*1NapCH$_2$CH$_2$CO-Aib*[K*Nle*ADD]*Nle* -NH$_2$	955.66	955.48	16.72
44	Ac-*1NapCHCHCO-Aib*[KFADD]*Nle* -NH$_2$	953.46	953.85	16.95
45	Ac-*1NapOCH2CO-Aib*[K*1Nal*ADD]*Nle* -NH$_2$	1028.88	1028.51	16.61

HPLC conditions: Phenomenex C18 column, 5μm 100 Å 4.6×250 mm, 214 nm, Solvent A=0.1% TFA in H$_2$O, Solvent B=0.1% TFA, 10% H$_2$O in acetonitrile. Gradient: 0% B to 100% B over 30 min).